IV. DISCUSSION AND RESULT

We find from Tables III and II, that a satisfactory value of the $1/e$ width is obtained for $\mu\sim1.12$, except in the case of Al. The agreement of the calculated difference in $1/e$ width for electron and positron multiple scattering (Table IV) with the experimental results also seems fairly satisfactory for $\mu\sim1.12$, though we are comparing slightly different quantities. The fact that $\mu\sim1.8$, the value found to fit the experimental data of Hanson *et al.*[8] for the $1/e$ width for 15–16 Mev electron multiple scattering by Au and Be in paper A, gives low results for electron scattering around 1 Mev seems to suggest that the screening parameter, λ, is probably somewhat energy dependent.

[8] A. O. Hanson, L. H. Lanzl, E. M. Lyman, and M. B. Scott, Phys. Rev. 84, 634 (1951).

PHYSICAL REVIEW VOLUME 121, NUMBER 6 MARCH 15, 1961

Nuclear Quadrupole Absorption in Indium Metal*†

W. W. Simmons‡ and C. P. Slichter§
Department of Physics, University of Illinois, Urbana, Illinois

(Received November 7, 1960)

The nuclear quadrupole resonance spectrum of indium metal has been observed and studied over the temperature range 4°K to 225°K. The four transition frequencies occur in ratios of 1:2:3:4, as expected from the crystal structure of indium. The lowest transition at 1.881 Mc (at 4.2°K) gives a quadrupole coupling constant of (45.19±0.02) Mc.

The root second moment of 18 kc is substantially greater than the 4 kc predicted from magnetic dipolar coupling among the nuclei, is temperature independent, but is somewhat sample dependent. It is shown that for a pure quadrupole resonance, the pseudo-exchange coupling produces an exchange broadening. This mechanism is shown to contribute about 10 kc to the root second moment and predicts a Gaussian line shape, as observed. It is concluded that in some cases magnetic impurities must be present, but it is not known whether or not the narrowest line represents a natural width.

The field gradient is computed assuming point ions and a uniform electron density by a technique that converges rapidly with distance, but the answer is too small by a factor of 3. It is argued that it is important to consider the p valence electrons. The temperature dependence of frequency is very strong (a 23% decrease between 4°K and 220°K), and unexplained. It appears to show that the field gradients cannot be computed assuming point ions and a smooth charge distribution.

A resonance in the superconducting state is reported.

I. INTRODUCTION

PURE quadrupole resonance may be observed in a solid when a nucleus possessing a quadrupole moment is situated in a lattice having lower than cubic symmetry. This paper reports the observation and study of the nuclear quadrupole resonance spectrum in indium metal. During the course of this research, Knight and Hewitt independently observed the same resonance. A preliminary report of their work has been published.[1]

We will center our attention on three principal issues. These are: (1) the interpretation of the shape and breadth of the resonance lines; (2) calculation of the axial field gradient at the nuclear site; (3) the temperature dependence of this field gradient. In addition, an observation of the resonance below the superconducting transition temperature ($T_c=3.39$°K) is reported.

A general theory of line shape for pure quadrupole resonance has not as yet been developed. However, it is well known that nuclear resonance line widths are in general somewhat broader, for heavier elements, than would be expected on the basis of dipolar coupling alone. We account for much of the observed line breadths in indium phenomenologically in terms of the pseudo-exchange interaction.[2,3] On account of the large spin of the indium, we show that we have a case of exchange broadening rather than exchange narrowing. The exchange interaction constant A_{ij} is scaled from the thallium data of Bloembergen and Rowland.[3] To the extent of this approximation, the line shapes are shown to be Gaussian. Pseudo-exchange will lead to broadening in a large-spin, pure quadrupole resonance experiment, since a given neighboring pair of nuclei in general will not be able to conserve energy by a mutual spin flip. In addition, it appears that impurities may in some instances play important roles in determining line breadths.

An analysis of the effect of the magnetic modulation field on the resonance will be given. For the condition that this field is small in comparison with the natural resonance line width, this analysis will lead to a simple interpretation of the second moment and shape of the resonance line. Comparison of the results of this

* Based on a thesis (W. W. Simmons) submitted in partial fulfillment of the requirements for the degree of Doctor of Philosophy.

† This research supported jointly by a grant from the Alfred P. Sloan Foundation and the U. S. Atomic Energy Commission.

‡ Now at Space Technology Laboratories, Inc., Los Angeles, California.

§ Alfred P. Sloan Fellow.

[1] R. R. Hewitt and W. D. Knight, Phys. Rev. Letters 3, 18 (1959).

[2] M. A. Ruderman and C. Kittel, Phys. Rev. 96, 99 (1954).

[3] N. Bloembergen and T. J. Rowland, Phys. Rev. 97, 1679 (1955).

analysis with experimental recorder tracings will be discussed.

At the present time, no detailed, exact treatment of crystalline field gradients is possible, due primarily to a lack of accurate electronic wave functions for the crystal. In terms of a simple model of charge distribution, Cohen and Reif[4] have set forth an expression for the field gradient at a particular nucleus (at the origin). This expression is

$$eq=(1+R_s)eq_v+(1+\gamma_\infty)eq_i, \quad (1)$$

where q_i represents the field gradient due to all atoms at lattice states external to the origin, γ_∞ is the Sternheimer antishielding factor for the solid, representing the polarization of the closed electronic shells surrounding the origin, q_v is the field gradient arising from the p part of the atomic orbital wave function describing the valence electrons centered primarily at the origin, and R_s is the core correction factor for the solid. Previous calculations of q_i for ionic crystals[5–7] have approximated the external atoms by point charges at the lattice sites, evaluating q_i by a direct sum of $[P_2(\cos\theta_j)/r_j^3]$ over all points j within a sphere of radius much greater than the interatomic distance. The same technique is applicable to metals if one assumes a uniform distribution of conduction electrons. However, convergence of this sum is, in general, very poor. We will present an alternative method for calculating q_i; essentially, the metal is partitioned into the electrically neutral Wigner-Seitz cells. Assuming a uniform distribution of conduction electrons throughout each cell, q_i is evaluated by a sum over the multipole moment contribution of each external cell. Convergence of this sum is much more rapid. A simple physical argument shows why the two methods, which seem on the surface to be similar, actually are quite different.

The remaining terms in expression (1) can only be approximately obtained. The partial field gradient $(1+\gamma_\infty)q_i$ obtained from γ_∞ for the ion In^{+++} is too small (by approximately a factor 3.5) to account for the experimental value observed. This indicates that there is an appreciable contribution from the p part of the conduction electrons. Orders of magnitude for this contribution will be discussed.

A further test of the calculation of the quadrupole frequency is the measured dependence on temperature. The lattice constants a and c have been measured in indium from -183°C to $+135$°C by Graham, Moore, and Raynor.[8] In the approximation that the electron density is uniform (i.e., that there is no p character to the conduction electrons in the near vicinity to the nucleus so that $q_v=0$), the resonance frequency turns out to be proportional to $(c-a)/a^4$. Combining this expression with the measurements of Graham, Moore, and Raynor gives a temperature dependence much smaller than is observed. We suggest that one possible cause of the rapid temperature variation of the resonant frequency is to be found in consideration of the effect of the lattice distortion on the band structure through the term q_v. If this is true, the field gradient is due primarily to a p-like character of the conduction electrons close to the nucleus, and not to charges outside the Wigner-Seitz cell containing the nucleus as has been assumed for gallium and beryllium.

This paper will be presented in the following manner: In Sec. II, experimental details and methods of observing the nuclear resonance are given. In Sec. III, the frequencies and relative intensities of the observed resonance lines are given, together with a brief interpretation of these results. The experimental temperature dependence of the resonance frequencies is shown, but interpretation of the temperature dependence is deferred until Sec. VI. In Sec. IV, we discuss the line breadth and shape. Section V presents a calculation of the electric field gradient at the indium nucleus. In Sec. VI, we discuss the temperature dependence of the resonant frequency. In Sec. VII, the resonance in the superconductor is described.

II. EXPERIMENTAL METHODS

All resonance data reported in this work were obtained with a modified Pound-Knight-Watkins variable frequency spectrometer.[9] Two GL-6072 low-noise triodes[10] were used in place of the 6J6 oscillator tube. In addition, the voltage gain of the rf amplifier was increased, providing less susceptibility to microphonics and improvement in stability of oscillation amplitude and sensitivity when the oscillator was swept over a large frequency range.

Sinusoidal Zeeman (magnetic field) modulation was used to obtain a reference for phase-sensitive detection. Narrow banding was done with a conventional lock-in amplifier, operating with respect to a reference signal at twice the modulation frequency. The line shapes presented by the lock-in, for this modulation scheme, are essentially second derivatives of the true line shape.

Frequency measurements were made with a Hewlitt-Packard electronic counter. Resonance intensity measurements were made with the calibrator circuit of Watkins.[9]

The geometry of the cryostat system was such that the rf magnetic field was always oriented at right angles to the modulating field. Both the cryostat and

[4] M. H. Cohen and F. Reif, *Solid-State Physics*, edited by F. Seitz and D. Turnbull (Academic Press, New York, 1957), Vol. 5.
[5] R. Bersohn, J. Chem. Phys. **29**, 326 (1958).
[6] M. Pomerantz, thesis, University of California, 1958 (unpublished).
[7] R. A. Bernheim and H. S. Gutowsky, J. Chem. Phys. (to be published).
[8] J. Graham, A. Moore, and G. V. Raynor, J. Inst. Metals **84**, 86 (1955).
[9] R. V. Pound, *Progress in Nuclear Physics* (Pergamon Press, New York, 1952), Vol. 2, p. 21.
[10] T. Kushida, G. B. Benedek, and N. Bloembergen, Phys. Rev. **104**, 1364 (1956).

TABLE I. Comparison of experimental and theoretical frequencies and intensities.

Transition	Frequency (Mc) 4.2°K	77°K	Relative intensity $[I(I+1)-m(m+1)]$ Measured (77°K)	Predicted
$\nu_{1/2\to3/2}$	1.881	1.786	30	$24\times1.4=34$
$\nu_{3/2\to5/2}$	3.761	3.575	21.0	21
$\nu_{5/2\to7/2}$	5.642	5.364	12.4	16
$\nu_{7/2\to9/2}$	···	7.148	7.7	9

the modulating magnet have been described elsewhere.[11] Temperatures were measured over various ranges with a calibrated carbon resistor, a copper-constantan thermocouple, and a Bourdon pressure gauge. The resonant frequency as a function of temperature was obtained by repeated sweeps through the resonance as the sample warmed gradually; static temperature check points were provided by liquid helium (4.2°K), liquid nitrogen (77°K), and dry ice (194.5°K).

Samples of indium metal used throughout the bulk of the experiment were 99.96% indium powder supplied by the A. D. Mackay Company, sifted through a 400-mesh sieve. As will be discussed later, our line widths show a substantial sample dependence. Typical particles are roughly spherical and about 10–15μ mean diameter.

III. RESONANCE FREQUENCIES AND INTENSITIES

The quadrupolar interaction in general may be written[4]

$$H_Q=\sum_m Q_m(\nabla E)_{-m},$$

where the sum is over the five irreducible components of the nuclear quadrupole moment tensor Q_m and the electric field gradient tensor $(\nabla E)_{-m}$. For indium metal, the crystal structure is face-centered tetragonal, the basic cell having the dimensions a, a, and $c=1.078a$ at room temperature. Therefore, each nuclear site is equivalent. The principal axes of (∇E) correspond to X, Y, and Z along the crystal directions (1,0,0), (0,1,0), and (0,0,1). Further, with this choice of axes, the fourfold rotational symmetry of the crystal about the z axis permits (∇E) to be described by a single parameter equation. Thus,

$$H_Q=[(eq)(eQ)/4I(2I-1)](3I_Z^2-I^2), \quad (2)$$

giving the energy levels

$$E_m=[e^2qQ/4I(2I-1)][(3m^2-I(I+1)], \quad (3)$$

in a representation in which I_Z is diagonal. In these equations, eQ is the (scalar) electric quadrupole moment of the nucleus, $eq=\partial^2V/\partial Z^2$ is the axial component of the electric field gradient, V is the electrostatic potential at the nucleus, and I is the nuclear spin.

[11] L. C. Hebel, thesis, University of Illinois, 1957 (unpublished).

For $I=9/2$, there are four distinct $\Delta m=\pm1$ transitions, having resonant frequencies

$$\nu_{|m|\to|m|+1}=(2|m|+1)3A/h, \quad (4)$$

where $A=e^2qQ/4I(2I-1)$.

Observed resonance frequencies for the various transitions are listed in Table I, for the fixed temperatures 4.2°K and 77°K. It is seen that the frequency ratios are closely 1:2:3:4, in agreement with Eq. (4). The values listed are, in each case, averages for several runs.

Relative intensities are also shown, as measured by the calibrator. A discussion of the calibrator operation appears in Appendix A. The observed intensities are normalized to 21 for the $\nu_{|3/2|\to|5/2|}$ transition. The transition $\nu_{|1/2|\to|3/2|}$ is a special case; the extra multiplying factor (1.4) appears from the degeneracy of the $m=\pm1/2$ levels.

These frequencies lead to a quadrupolar coupling constant at 4.2°K,

$$|e^2qQ/h|=(45.19\pm0.02)\text{ Mc},$$

in good agreement with Knight's value[1] (45.24±0.02) Mc/sec. The sign of the field gradient eq cannot be determined from this experiment.

Typical signal-to-noise ratios are shown by the recorder tracings in Fig. 1.

IV. RESONANCE LINE SHAPES AND WIDTHS

The resonance line-breadth in indium is substantially broader than can be accounted for by the dipolar coupling of a nucleus to its neighbors. Such a mechanism contributes less than 4 kc to the root second moment which is experimentally about 18 kc. In heavy metals (notably Ag and Tl), the predominant mechanisms determining magnetic resonance linewidths are second order processes involving interactions between a conduction electron and the nuclear spin. The theory of pseudodipolar and pseudo-exchange coupling in metals has been given independently by Rudermann and Kittel,[2] and Bloembergen and Rowland.[3] The pseudo-exchange interaction is

$$H_{\text{ex}}=\sum_{j>i}A_{ij}\mathbf{I}_i\cdot\mathbf{I}_j, \quad (5)$$

where

$$A_{ij}\propto\gamma_i\gamma_j|\psi_i(0)|^2|\psi_j(0)|^2/E_F,$$

E_F is the Fermi energy for the metal, γ the nuclear gyromagnetic ratio, and $|\psi(0)|^2$ is the probability density evaluated at the nucleus for an s electron at the Fermi surface.

Ordinarily the pseudo-exchange coupling contributes to line-broadening only between unlike nuclei. As we show below, however, it produces broadening of a pure quadrupole resonance.

It is possible to compute the coupling constant for indium metal $(A_{ij})_{\text{In}}$ from the known value for thallium metal of 15.5 kc. To do this scaling, we assume that

the Fermi energies of the metals are the same, and that the ratio of the hyperfine interactions In to Tl in the metal is the same as that for the free atom. The latter we obtain from applying a well-known formula[12] to the $Tl^{++}-6s$ and $In^{++}-5s$ states. The resulting estimate is $(A_{ij})_{In}/h \cong 0.75$ kc.

Shulman has suggested to us that this interaction constant may also be scaled in a different manner. The In^{115} and Sb^{121} dipolar resonances in the semiconductor InSb are broadened by indirect exchange. Shulman *et al.*[13] give the contributions of H_{ex} to the second moments of the magnetic resonance lines,

$$\langle \Delta H_2^2 \rangle_{ex} = 62 \pm 4 \text{ gauss}^2 \text{ for } InSb^{121};$$

$$\langle \Delta H_2^2 \rangle_{ex} = 22 \pm 1 \text{ gauss}^2 \text{ for } In^{115}Sb.$$

Applying the second moment formula of Van Vleck[14]

$$\sigma_i = \tfrac{1}{3} \sum_j I_j(I_j+1) A_{ij}^2/h^2 = (\gamma_i^2/2\pi)(\Delta H_{2i}^2)_{ex}, \quad (6)$$

where the subscripts i and j refer to distinct nuclear species, the interaction magnitude for four nearest neighbors of type j is $|A_{ij}|/h = 1.3$ kc. These two estimates are of the same order of magnitude.

One would expect the indirect exchange interaction to be approximately the same in both the semiconductor and the metal. The reason is that the energy gap in the semiconductor is small in comparison with the width of the energy bands. In either the metal or the semiconductor, the second order interaction involves a virtual transition of an electron to a higher, unoccupied energy state. Therefore, the assumption is made that the presence of the gap is only a minor perturbation on the strength of the interaction (which is proportional to the number of electron states available). In particular, if the Fermi energies in the metal and in the semiconductor (as measured from the bottom of the filled band) are about equal, then the equivalent magnetic field seen by a Sb^{121} nucleus due to a single In^{115} neighbor should be about the same as the field seen by an In nucleus in the metal due to a single In^{115} neighbor.

We will now establish a basis for computing an approximate line shape. We shall see that the fact that the spin of indium is quite large enables us to regard the pseudo-exchange interaction as a magnetic field at nucleus (i), due to nucleus (j), interacting with the dipole moment of (i). This approximation will be referred to as the "large spin" approximation.

We assume that the pseudo-exchange interaction is much larger than the pseudo-dipolar interaction in indium. The pseudo-exchange interaction may be written

$$H_{ex} = \sum_{j>i} A_{ij}[I_{iz}I_{jz} + \tfrac{1}{2}(I_{i+}I_{j-} + I_{i-}I_{j+})]. \quad (7)$$

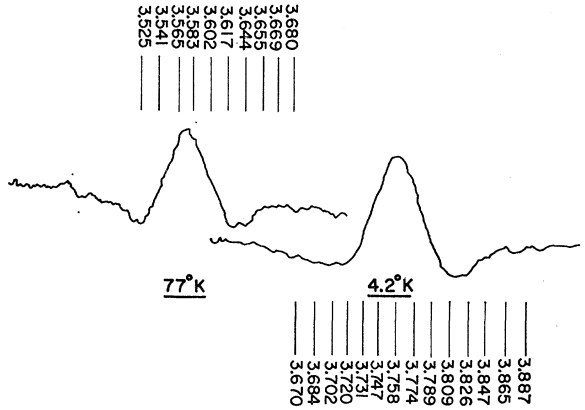

FIG. 1. Experimental recorder tracings as a function of frequency at 4.2°K and 77°K. Modulation field is 40 gauss peak-to-peak sinusoidal. Time constants were 5 sec at 4.2°K and 10 sec at 77°K. Frequencies are indicated in Mc.

In considering the effect of this interaction on the second moment, we ignore matrix elements which do not conserve energy between initial (m_i,m_j) and final (m_i',m_j') nuclear spin states. From the quadratic dependence of energy levels E_m upon m [Eq. (3)], it is evident that the partial interaction $\frac{1}{2}(I_{i+}I_{j-}+I_{i-}I_{j+})$ only connects states $m_i=m$, $m_j=m\pm1$ with $m_i'=m\pm1$, $m_j'=m$. For $I=9/2$, there are 18 possible combinations. On the other hand, the partial interaction $I_{iz}I_{jz}$ connects all possible $(2I+1)^2=100$ states of spins (i) and (j). Since the spin orientation of a given pair of nuclei is random, neglecting the $(I_{i+}I_{j-}+I_{i-}I_{j+})$ part of H_{ex} may lead to an underestimate of the interaction by $\cong 20\%$. One notes that the accuracy of the approximate form

$$H_{ex} \cong \sum_{j>i} A_{ij}I_{iz}I_{jz} \quad (8)$$

increases with increasing spin. Also, the terms neglected by Eq. (8) are just those giving rise to exchange narrowing of a magnetic resonance line.

Within the context of the large spin approximation, $H_{ex} \cong \sum_{j>i} A_{ij}I_{iz}I_{jz}$ is equivalent to a static magnetic field, of magnitude $A_{ij}I_{jz}/\gamma\hbar$, acting in the z direction on spin (i) due to spin (j), and independent of m_i. For 12 nearest neighbors, the mean square value of this field is

$$\text{Trace}\left[\frac{12A_{ij}^2I_{jz}^2}{(\gamma\hbar)^2}\right] = \text{Trace}\left[\frac{12|A_{ij}|^2}{\gamma^2\hbar^2}\left(\frac{I^2}{3}\right)\right] = \frac{|A_{ij}|^2}{\gamma^2\hbar^2}4I(I+1), \quad (9)$$

resulting in the mean square frequency width

$$\sigma_{|m|} = (|A_{ij}|^2/h^2)4I(I+1) \quad (10)$$

for *all* transitions $\nu_{|m|\to|m|+1}$.

To establish the line shape, we consider the energy levels to be determined only by the quadrupolar

[12] See, for example, H. E. White, *Introduction to Atomic Spectra* (McGraw-Hill Book Company, New York, 1934), p. 363.
[13] R. G. Shulman, B. J. Wyluda, and H. J. Hrostowski, Phys. Rev. **109**, 808 (1958).
[14] J. H. Van Vleck, Phys. Rev. **74**, 1168 (1948).

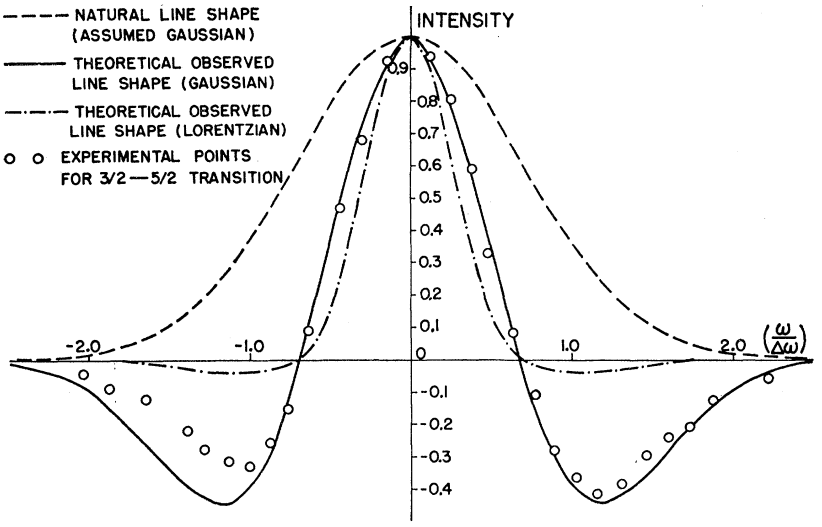

FIG. 2. Experimental and theoretical plot of nuclear signal from lock-in amplifier as a function of reduced frequency $(\omega/\Delta\omega)$.

interaction and by the large spin pseudo-exchange interaction. Using Eqs. (4) and (8), we find the transition frequency of spin (i) in the presence of spin (j) is

$$\nu_{|m_i|\to|m_i|+1}=(E_{|m_i|+1,\,m_j}-E_{|m_i|,\,m_j})/h$$
$$=(3A/h)(2|m_i|+1)+(A_{ij}/h)m_j. \quad (11)$$

We assume that all $(2I+1)$ values of m_j are equally probable. Letting $\nu_j=A_{ij}m_j/h$ be the contribution to the shift of $\nu_{|m_i|\to|m_i|+1}$ from the value $3A(2|m_i|+1)/h$ due to the (j) nucleus, the frequency shift due to all nuclei in the crystal other than (i) is

$$\nu=\textstyle\sum_j \nu_j=\sum_j (A_{ij}/h)m_j. \quad (12)$$

We now apply the general method described by Cohen and Reif.[15] If now $P_j(\nu_j)d\nu_j$ is the probability that ν_j lies in the range $d\nu_j$, then the probability $g(\nu)d\nu$ that ν lies in the range $d\nu$ is

$$g(\nu)=\prod_j \int [P_j(\nu_j)\delta(\nu-\sum_j \nu_j)d\nu_j]. \quad (13)$$

We assume that $P_j(\nu_j)$ is constant over the range $-IA_{ij}/h=-a<\nu_j<a=IA_{ij}/h$. This assumption is not strictly valid. Nevertheless, the dipolar interaction broadens each of the ten satellites sharply defined by $A_{ij}m_j/h$. If dipolar broadening is of order A_{ij}/h, then our assumption is very good.

Evaluation of expression (13) for 12 nearest neighbors, using the relations

$$P_j(\nu_j)=1/2a;$$
$$\delta(\nu-\sum_j \nu_j)=\frac{1}{2\pi}\int_{-\infty}^{\infty} \exp[i(\nu-\sum_j \nu_j)\tau]d\tau,$$

gives

$$g(\nu)=\frac{1}{2\pi}\int_{-\infty}^{\infty}\left(\frac{\sin a\tau}{a\tau}\right)^{12} e^{i\nu\tau}d\tau. \quad (14)$$

[15] M. H. Cohen and F. Reif, *Solid-State Physics*, edited by F. Seitz and D. Turnbull (Academic Press, Inc., New York, 1957), Vol. 5, p. 368.

The function $(\sin a\tau/a\tau)^{12}$ is the Fourier transform of $g(\nu)$. Evaluation of the integral by contour integration leads to a shape function which is very closely Gaussian. We therefore approximate it by

$$g(\nu)=\frac{1}{(2\pi\sigma)^{\frac{1}{2}}}\exp[\nu^2/2\sigma]. \quad (15)$$

In this expression, σ is the second moment. It may be evaluated from the coefficient of $(\tau^2/2!)$ in the expansion

$$\left(\frac{\sin a\tau}{a\tau}\right)^{12}=\left[\sum_{n=1}^{\infty}(-1)^{n-1}\frac{(a\tau)^{2n-2}}{(2n-1)!}\right]^{12} \quad (16)$$

to be

$$\sigma=(|A_{ij}|^2/h^2)4I^2. \quad (17)$$

Using the previously estimated value $|A_{ij}|/h\approx 1$ kc, one obtains $\sqrt{\sigma}\approx 10$ kc for all transition frequencies $\nu_{|m|\to|m|+1}$.

For the upper three transitions $\nu_{3/2\to5/2}$, $\nu_{5/2\to7/2}$, $\nu_{7/2\to9/2}$, and for small modulation fields $H_0\sin\Omega t$, the lock-in amplifier presents the second derivative of the resonance line $S_{|m|}$ which is proportional to

$$\left[1-\frac{(\nu-\nu_0)^2}{\sigma}\right]\exp\left[-\frac{(\nu-\nu_0)^2}{2\sigma}\right], \quad (18)$$

where ν_0 is the frequency of the center of the line. For the lowest transition $\nu_{1/2\to3/2}$, the shape presented is more complicated, due to the degeneracy of the energy levels $E_{\pm\frac{1}{2}}$ for a magnetic field H_0 applied at a general angle θ_z to the tetragonal crystal axis z.

The experimental line shapes are distinctly Gaussian, as demonstrated in Fig. 2. A Lorentzian line shape, fitted at the peak and at the points where the tracing crosses the baseline, is shown for comparison. The dependence of $S_{|m|}$ on $(H_0)^2$ is shown in Fig. 3.

For $(\gamma H_0/2\pi)^2\ll\sigma$, the second moment σ is given by

TABLE II. Experimental linewidths and second moments.

Transition	Sample A $\Delta\nu$ (kc)	Sample A $\sigma^{\frac{1}{2}}$ (kc)	Sample B $\Delta\nu$ (kc)	Sample B $\sigma^{\frac{1}{2}}$ (kc)
$\nu_{9/2\to7/2}$	35±2	33	20±2	16
$\nu_{7/2\to5/2}$	37±2	35	22±2	18
$\nu_{5/2\to3/2}$	34±2	32	23±2	19

the square of the frequency separation $\Delta\nu$ between the peak frequency ν_0 and the baseline crossover frequency. For larger H_0, the first order correction formula, for the upper three transitions, is

$$\sigma\simeq\Delta\nu^2\left(1-\frac{3}{14}\frac{(\gamma H_0/2\pi)^2}{\Delta\nu^2}\right). \tag{19}$$

The observed line shape is not appreciably affected by the size of H_0.

Observed linewidths are independent of temperature, in agreement with the postulated broadening mechanism H_{ex}. However, measurements of σ have shown a strong sample dependence. Within material from the same lot, values of σ showed no sample dependence. In a conversation with Knight, he reported narrower lines than we had observed. Subsequent measurements were made on a sample taken from a different lot, presumably of the same purity material; measured values of σ were found to be smaller by about 30%. Spectrochemical analyses of impurity concentrations have not been consistent, but tend to indicate that neither sample is as pure as quoted by the manufacturer. Whether or not the impurities are in the bulk material or on the particle surfaces is not known.

Table II shows $\Delta\nu$ and σ for the upper three transitions. These data were taken at 77°K, with a modulating field $H_0\simeq20$ gauss. The approximation (19) represents a slight underestimate of σ for H_0 this large. Frequencies are given in (kc).

Our computed root second moment of about 10 kc is too small by a factor of two. It would be increased somewhat by inclusion of contributions from other than nearest neighbors. Possibly a larger value of A_{ij} is needed.

Note that the resonance linewidths are not determined by a quadrupolar interaction, since all transitions show approximately the same width (for a given specimen). In addition, annealing the samples for various times did not affect the linewidths.

One possible explanation of the sample dependence is the presence of magnetic impurities, such as transition elements. One would expect them to possess only the time-average electronic moment as observed, for example, by Sugawara[16] in alloys of transition elements in copper. If this moment varied with temperature according to a Curie-Weiss law (a reasonable assumption for many paramagnetic impurities), the line-breadth would be temperature dependent, in contradiction to the facts. On the other hand, if there were small ferromagnetic particles imbedded in the sample, the line-breadth would be independent of temperature, the same for all transitions, and sample dependent. It is not unreasonable that the line shape might be Gaussian.

[16] T. Sugawara, J. Phys. Soc. Japan **14**, 643 (1959).

V. THEORY OF QUADRUPOLE RESONANCE FREQUENCIES

The crystal structure of indium has been described in Sec. III. Choosing a nucleus at the origin of the set of crystalline axes xyz previously defined, the axial field gradient component at that nucleus is

$$eq_{zz}=eq=\int\rho(\mathbf{r})\left(\frac{3z^2-r^2}{r^5}\right)d\mathbf{r}, \tag{20}$$

where $\rho(\mathbf{r})$ is the electric charge density at the point $\mathbf{r}$ excluding the nucleus at the origin. As a first approximation, we assume

$$\rho(\mathbf{r})=\rho_e+Ze\sum_i\delta(\mathbf{r}-\mathbf{r}_i), \tag{21}$$

where ρ_e is a constant representing the (assumed) uniform distribution of conduction electrons, and the term $Ze\sum_i\delta(\mathbf{r}-\mathbf{r}_i)$ represents the charge density of the ionic cores, treated as point charges at the lattice sites. Z is taken to be 3, the normal valence of indium. We temporarily neglect the Sternheimer polarization of the closed electronic shells surrounding the origin.

Expression (20) has been evaluated by two methods. The first method makes immediate use of the relation

$$\int\rho_e\left(\frac{3z^2-r^2}{r^5}\right)d\mathbf{r}=0, \tag{22}$$

when integrated over a sphere of radius R. The remaining expression,

$$eq=(Ze)\sum_i\left(\frac{3z_i^2-r_i^2}{r_i^5}\right), \tag{23}$$

is evaluated by a direct machine sum[17] over all lattice points within the sphere R. Convergence of the sum is exceedingly slow, since it depends upon the *angular* averaging to zero of $(3z_i^2-r_i^2)$ for a spherical shell containing many lattice points at a distance $r_i\gg a$ (a=lattice constant). For approximately 62 000 lattice points ($R>14a$), the result is $eq=(-0.349)Ze/a^3$, with contributions from preceding individual shells still contributing about 2% of the total.

The second method converges much more rapidly, since it depends upon charge cancellation of negative conduction electrons and positive ionic cores for distances far from the origin. We partition the metal into atomic cells (the Wigner-Seitz polyhedra); each

[17] The authors are indebted to Mr. D. Markowitz for programming the IBM 650 for this calculation.

of these cells is electrically neutral. The field gradient due to conduction electrons in the cell centered at the origin is evaluated directly; the contribution from the remaining cells is evaluated by a multipole moment expansion of the potential $\Phi(x,y,z)$:

$$\Phi(x,y,z)=\sum_i \int_{\text{cell}} d\mathbf{R}\rho(\mathbf{R}) \times \sum_{n=0}^{\infty}\left[\frac{1}{n!}\left(\frac{x\partial}{\partial x'}+\frac{y\partial}{\partial y'}+\frac{z\partial}{\partial z'}\right)^n \frac{1}{|\mathbf{r}'|}\right]_{\mathbf{r}'=\mathbf{r}_i},$$

where the integral is over the Wigner-Seitz (W-S) cell, and the sum over i includes all such polyhedra in the crystal. $\mathbf{r}_i$ is the vector to the ith lattice site, and $\mathbf{R}=\mathbf{r}-\mathbf{r}_i$. The field gradient due to these cells is $\partial^2\Phi/\partial z_i^2$. The charge density is taken to be

$$\rho(\mathbf{R})=\rho_e+Ze\delta(\mathbf{R}),$$

subject to the condition that

$$\int_{\text{cell}} \rho(\mathbf{R})d\mathbf{R}=0.$$

Details of the calculation appear in Appendix II. Since both the monopole and dipole moments vanish for the Wigner-Seitz cells, the lowest nonvanishing multipole is the quadrupole. The contribution to the field gradient with increasing radii of neighbor shells proceeds toward zero as $1/r_i^2$; convergence is even more rapid for higher order multipoles.

The net result of the calculation, for the first three neighbor shells and for the 2-pole, 4-pole, and 6-pole moments is

$$eq=(-0.319)Ze/a^3.$$

This result is within 10% of the machine calculated value (20).

Since both methods of calculation are apparently the same, one might wonder why their convergence is so different. The answer is most easily seen by realizing that the sphere of radius R includes complete W-S cells in its interior, but on its surface it includes fractional cells. The fractional W-S cells included at the surface all have nonvanishing monopole moments, and their contribution is thus slowly convergent with R. Note, moreover, that if one is near to the physical surface in a real material, the surface will be important in producing a gradient only to the extent that the individual cells have nonvanishing monopole or dipole moments. Otherwise, the surface effects are very short range.

The effect of the closed electronic shells surrounding the origin is described by a multiplicative constant γ_∞ (Sternheimer antishielding factor). γ_∞ has been calculated for several heavy ions[18–20]; indium has not been included. An empirical interpolation from calculated values for other ions gives the probable γ_∞ for In^{3+}, $-25<\gamma_\infty<-15$. Assuming that $\gamma_\infty=-20$ is representative, and that the ion value is applicable in the solid, the field gradient becomes

$$eq=(1-\gamma_\infty)(-0.349)Ze/a^3=-1.09\times10^{14}\text{ esu},$$

where $a=4.59$ A and $Z=3$. This field gradient value gives the quadrupolar coupling constant

$$|e^2qQ/h|_{\text{ionic}}=9.2\text{ Mc}$$

at room temperature, to be compared with the experimental value (extrapolated from Fig. 4)

$$|e^2qQ/h|=30\text{ Mc}.$$

It is clear that we have a correct order of magnitude estimate of eq. Detailed agreement on the basis of this ionic model is poor. The chief drawback of the above calculations lies in the simple assumption that the conduction electron charge density is uniform throughout the neighborhood of the origin. The field gradient is quite sensitive to any p-wave admixture in the conduction electron wave function, due to the deeply penetrating p orbital; in other words, $\langle 1/r^3\rangle$ is quite large.

In the free atom, atomic beam measurements give an accurate knowledge of the quadrupolar coupling constant. The field gradient at the nucleus for an electron in a p orbit directed along the x axis is [21]

$$eqQ=1123\text{ Mc}.$$

In a cubic crystal, no field gradient appears at the nucleus. To the extent that cubic symmetry is destroyed, the cubic symmetry of the p-electron distribution is also destroyed; that is, the p electrons now spend a different amount of time, on the average, in the z direction than in the x and y directions.

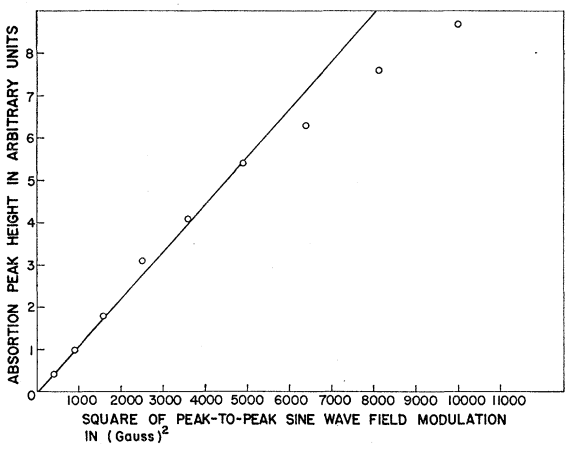

FIG. 3. Nuclear signal from lock-in amplifier versus the square of the field modulation amplitude. Note the departure of the signal height from the relation $S\propto H_0^2$ as $(\gamma H_0/2\pi)$ approaches the linewidth σ.

[18] R. M. Sternheimer and H. M. Foley, Phys. Rev. **102**, 731 (1956).
[19] T. P. Das and R. Bersohn, Phys. Rev. **102**, 733 (1956).
[20] G. Wikner and T. P. Das, Phys. Rev. **109**, 360 (1958).
[21] A. K. Mann and P. Kusch, Phys. Rev. **77**, 427 (1950).

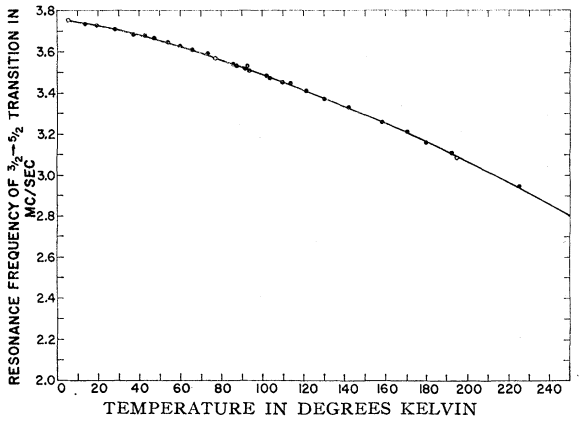

FIG. 4. Temperature dependence of the resonance frequency. These data were taken for the $\nu_{3/2\to5/2}$ transition. Open circles represent frequencies obtained at fixed temperatures.

Since the coupling at room temperature is only about 3% of the coupling for a single p orbit directed along the x axis, we see that we can account for the experiments with only a small disturbance from cubic symmetry. It is interesting to note that the fractional lattice distortion $\delta=c/a-1$, of 7.8% is comparable to the p-electron unbalance needed. We are tempted, then, to postulate that

$$\nu=c\nu_0\delta,$$

where ν_0 is the frequency of a single unbalanced p electron, and c a constant of order unity. Were the lattice cubic, $\delta=0$ and the quadrupole frequency would vanish. Unfortunately, the temperature dependence of ν suggests that $\nu=c\delta^n\nu_0$, where $n\cong4$. In this case, c must be a very large number. A detailed band theory calculation is necessary to evaluate accurately the p-electron contribution. Note that p electrons may contribute to the field gradient in metals without the postulate of a certain fraction of covalent bonding, as is necessary for evaluating field gradients in ionic and covalent crystals. We strongly suspect that the p-electron unbalance is the principal source of the quadrupole splitting.

VI. TEMPERATURE DEPENDENCE

The temperature dependence of the frequency (Fig. 4) has been measured from 4°K to 220°K. Over this interval, it decreases 23%, a fractional change much greater than that found for pure quadrupole resonances in molecular crystals which are typically 2% over such a range.

The calculation of the field gradient in the previous section supposed all the atoms to be at rest. Thermal vibrations may affect results in two ways. First of all, since the computed field gradients actually fluctuate in time and since the rate is rapid compared to the nuclear resonance frequencies, we should average our answer over time. Secondly, the thermal vibrations produce changes in the lattice dimensions, so that the time-average dimensions are functions of temperature.

The former effects are important in explaining the temperature dependence of the resonant frequency for molecular crystals. They can be estimated for a calculation such as that in the preceding section by assuming that the gradient is due to six charges located at $(\pm a, 0, 0)$, $(0, \pm a, 0)$, and $(0, 0, \pm c)$. The fractional correction to the frequency is then found to be of order $\langle\Delta x^2\rangle_{\rm av}/a^2$, where $\langle\Delta x^2\rangle_{\rm av}$ is the time average of the relative displacement of two neighboring atoms due to lattice vibrations. This effect is much too small to account for the observed changes.

Graham, Moore, and Raynor have measured the lattice constants of indium from 90°K to 408°K. They find

$$a=4.5422(1+2.59\times10^{-5}T+1.15\times10^{-10}T^3),$$
$$c=4.9141(1+2.59\times10^{-5}T-1.15\times10^{-10}T^3),$$
$$c/a=1.0819(1-2.30\times10^{-10}T^3),$$

where T is the temperature in degrees Kelvin.

Since δ is much more strongly temperature dependent than either c or a, we may concentrate our attention on it. Between 100°K and 250°K, δ drops from 8.17×10^{-2} to 7.80×10^{-2}, a 5% decrease, while ν drops from 3.48 Mc to 2.80 Mc, a 20% decrease. If $\nu=c\delta^n$, this implies $n\cong4$, a very strong dependence. O'Sullivan, Robinson, and Simmons[22] have extended the temperature dependence of ν to the melting point of indium (429°K), using a super-regenerative receiver to detect $\nu_{|7/2|\to|9/2|}$.

Among other measurements, they obtain

$$\nu|7/2|\to|9/2|=5.01\text{ Mc},\quad T=300°\text{K},$$
$$\nu|7/2|\to|9/2|=3.13\text{ Mc},\quad T=428°\text{K}.$$

Their results indicate that, if $\nu=c\delta^n$, then the relation ($n=$constant) cannot be made to fit the data over the entire temperature range (4–429°K). It is certainly clear that our simple calculations based on ion cores and uniform electron distributions are inadequate to account for the temperature dependence. About the only feature which is correct is that the frequency decreases as the lattice becomes more cubic.

If the field gradient arises from unbalanced p electrons, a band-theory calculation is needed. Judging by the work of Harrison on aluminum, a metal which is isoelectronic with indium but cubic, we expect the second Brillouin zone to be partly filled. The zone structure for the indium lattice will be distorted from that of a face-centered cubic. If the Fermi surface is near the zone boundary, as is the case for aluminum, it may be that the lattice distortion produces rather marked redistributions of the electrons in $\mathbf{k}$ space. Since it is reasonable to associate the p character with the direction of $\mathbf{k}$, a corresponding change in field

[22] W. J. O'Sullivan, W. A. Robinson, and W. W. Simmons, Bull. Am. Phys. Soc. 5, 413 (1960).

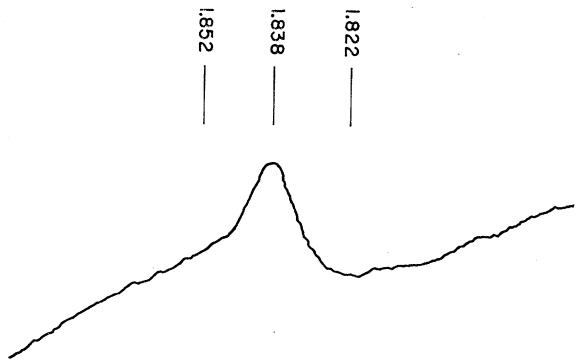

FIG. 5. Recorder tracing of the $\nu_{1/2\to3/2}$ transition in superconducting indium at 2.2°K. Frequency units are in Mc.

gradient would result. Lacking both wave functions and energies, we have not attempted a calculation, but two possible effects can be mentioned. The lattice distortion might distort the Fermi surface from a nearly spherical form, causing a redistribution of electrons. Or, even keeping the Fermi surface constant, the occupied volume in each band will be asymmetric in space for the asymmetric lattice [the Brillouin zone will be obtained from that of an fcc lattice by compressing the z coordinates of each point by a factor $1/(1+\delta)$]. Either of these two effects could give a very rapid variation of coupling with δ, but whether or not they provide a large enough effect, we cannot say.

VII. SUPERCONDUCTING RESONANCE

A tracing of the resonance ($\nu_{1/2}$) at 2.2°K (in the superconducting phase) is shown in Fig. 5. The strong baseline drift appears due to the modulation, and it is exceptionally strong when the sample is superconducting. This resonance was observed using the calibrator to buck out the spurious signal arising from the modulation.

An explanation for the asymmetrical line shape is not apparent. On account of this asymmetry, it is difficult to make an estimate of the linewidth.

If one assigns the peak frequency to be 1.84 Mc, then there is a shift in the resonance frequency from its value at 4.2°, 1.88 Mc, of approximately 2% downwards. Volume changes associated with the superconductivity phase transition are not, by several orders of magnitude, large enough to account for this large shift.[23] It does not seem likely that field gradients for nuclei near the particle surfaces should change by this much. The shift is much larger than that observed in superconducting gallium,[24] and in the opposite direction. The explanation of the large shift remains an open question at present.

APPENDIX I

The relative intensities of the resonance lines were measured using the calibrator. This device essentially places a large variable resistance in parallel with the tank circuit. When the resistance is varied by a small amount at the reference frequency, the tank impedance is also varied, just as is done by the nuclear signal. In practice, the input signal to the calibrator ϵ is directly proportional to the dc output voltage of the recorder as long as the input signal is small. ϵ is adjusted to cancel the nuclear signal at the peak of the resonance curve.

The total tank circuit conductance at resonance is then

$$G=G_0(1+4\pi\chi_{|m|}''Q\alpha)+G_1-\delta G_1,$$

where G_0 is the conductance of the LC circuit, $4\pi\chi_{|m|}''Q\alpha$ represents the fractional change in conductance due to the nuclear signal, Q is the coil quality factor, α is the effective filling factor, $\chi_{|m|}''$ is the equivalent nuclear susceptibility of the $\nu_{|m|\to|m|+1}$ transition, and $(G_1-\delta G_1)$ is the conductance of the calibrator.

Experimentally, one adjusts δG_1 so that

$$\delta G_1=(4\pi\chi_{|m|}''Q\alpha)G_0.$$

Since $\delta G_1\propto\epsilon$ and $G_0=1/Q\omega L$, for a given coil inductance one has $\epsilon\propto\chi_{|m|}''/\omega$.

Making use of the approximation

$$\chi_{|m|}''\simeq\frac{\pi}{2}\chi_0\frac{\omega_{|m|}}{\Delta\omega_{|m|}}\beta_{|m|},$$

where

$$\chi_0=N\gamma^2\hbar^2I(I+1)/3KT$$

and

$$\beta_{|m|}=3[I(I+1)-|m|(|m|+1)]/I(I+1)(2I+1),$$

one obtains

$$\epsilon\propto\beta_{|m|}/\Delta\omega_{|m|}.$$

Since the breadth of each transition $\Delta\omega_{|m|}$ is approximately the same,

$$\epsilon\propto[(99/4)-|m|(|m|+1)].$$

The relative intensities as read by the calibrator are therefore the ratios

$$(\epsilon)_{|9/2|}:(\epsilon)_{|7/2|}:(\epsilon)_{|3/2|}:(\epsilon)_{|1/2|}=9:16:21:24.$$

APPENDIX II

In Sec. V, the multipole moment expansion expression for the field gradient is

$$\frac{\partial^2\Phi}{\partial z_i^2}=\sum_i\int\rho(\mathbf{R})\sum_{n=0}^{\infty}\frac{1}{n!}\left[\frac{\partial^2}{\partial z_i^2}\left(x\frac{\partial}{\partial x_i}+y\frac{\partial}{\partial y_i}+z\frac{\partial}{\partial z_i}\right)^n\right]\times\frac{1}{|\mathbf{r}_i+\mathbf{R}|_{\mathbf{r}_i}}d\mathbf{R}, \quad (1a)$$

where the integral determining the multipole moments is chosen to be over the Wigner-Seitz polyhedron. This polyhedron for indium is a 12-sided figure bounded by the 12 planes

$$\pm x\pm y=\tfrac{1}{2}a;\quad \pm x\pm z/(1+\delta)=\tfrac{1}{2}a;\quad \pm y\pm 1/(1+\delta)=\tfrac{1}{2}a. \quad (2a)$$

When advantage is taken of the various symmetry

[23] G. D. Cody, Phys. Rev. **111**, 1078 (1958).
[24] R. H. Hammond and W. D. Knight, Bull. Am. Phys. Soc. 4, 452 (1959).

properties of the polyhedron, the integral expression for the l, m, p moment is

$$\langle x^l y^m z^p\rangle_{\rm av}=\int_0^{a/4} dy \int_y^{\frac{1}{2}a-y} dx \times \int_0^{(1+\delta)(\frac{1}{2}a-x)} dz(16\rho_e)x^l y^m z^p. \quad (3a)$$

Here ρ_e, evaluated from the condition that

$$\int(\rho_e+Ze\delta(\mathbf{R})d\mathbf{R}=0$$

when integrated over the polyhedron, is given by $\rho_e=-4Ze/ca^2$. The moments necessary for evaluation of $\partial^2\Phi/\partial z_i^2$ through $n=6$ are evaluated from the triple integral expression and tabulated below in terms of $1+\delta=c/a$.

$n=0$: All moments are zero, since $\int\rho(\mathbf{R})d\mathbf{R}=0$.

$n=1$: All moments are zero.

$n=2$: $\langle x^2\rangle_{\rm av}=\langle y^2\rangle_{\rm av}=\frac{1}{8}Ze(a/2)^2$; $\langle z^2\rangle_{\rm av}=\frac{1}{8}Ze(a/2)^2(1+\delta)^2$.

$n=3$: All moments are zero.

$n=4$: $\langle x^4\rangle_{\rm av}=\langle y^4\rangle_{\rm av}=\dfrac{3Ze}{80}(a/2)^4$; $\langle z^4\rangle_{\rm av}=\dfrac{3Ze}{80}(a/2)^4(1+\delta)^4$;

$$\langle x^2y^2\rangle_{\rm av}=\frac{7Ze}{720}(a/2)^4;\quad \langle x^2z^2\rangle_{\rm av}=\langle y^2z^2\rangle_{\rm av}=\frac{7Ze}{720}(a/2)^4(1+\delta)^2.$$

$n=5$: All moments are zero.

$n=6$: $\langle x^6\rangle_{\rm av}=\langle y^6\rangle_{\rm av}=\dfrac{85Ze}{5376}(a/2)^6$; $\langle z^6\rangle_{\rm av}=\dfrac{85Ze}{5376}(a/2)^6(1+\delta)^6$;

$$\langle x^4y^2\rangle_{\rm av}=\langle x^2y^4\rangle_{\rm av}=\frac{31Ze}{16128}(a/2)^6;\quad \langle x^4z^2\rangle_{\rm av}=\langle y^4z^2\rangle_{\rm av}=\frac{31Ze}{16128}(a/2)^6(1+\delta)^2;$$

$$\langle x^2z^4\rangle_{\rm av}=\langle y^2z^4\rangle_{\rm av}=\frac{31Ze}{16128}(a/2)^6(1+\delta)^4;\quad \langle x^2y^2z^2\rangle_{\rm av}=\frac{37Ze}{48384}(a/2)^6(1+\delta)^2.$$

Performing the derivatives indicated in Eq. (1a) leads to the expressions written below, through $n=6$. Some algebraic manipulation has been performed.

$$n=2:\quad \frac{\partial^2\Phi_2}{\partial z_i^2}=\frac{1}{2!}\frac{\delta}{2}(1+\tfrac{1}{2}\delta)(Ze/2)(a/2)^2\sum_i\frac{3}{r_i^5}\left(3-30\frac{z_i^2}{r_i^2}+35\frac{z_i^4}{r_i^4}\right).$$

$$n=4:\quad \frac{\partial^2\Phi_4}{\partial z_i^2}=\frac{1}{4!}\frac{21Ze}{8}(a/2)^4\sum_i\frac{1}{r_i^7}\left[\frac{x_i^4+y_i^4+z_i^4}{r_i^4}3\left(11\frac{z_i^2}{r_i^2}-1\right)+\left(1-3\frac{z_i^2}{r_i^2}-24\frac{z_i^4}{r_i^4}\right)+\frac{(8\delta+40\delta^2+36\delta^3+9\delta^4)}{14}\times\left(-5+105\frac{z_i^2}{r_i^2}-315\frac{z_i^4}{r_i^4}+231\frac{z_i^6}{r_8^6}\right)\right].$$

$$n=6:\quad \frac{\partial^2\Phi_6}{\partial z_i^2}=\frac{1}{6!}\frac{225Ze}{5376}(a/2)^6\sum_i\frac{1}{r_i^9}\Bigg\{17\Bigg[-875+10710\frac{z_i^2}{r_i^2}-10395\frac{z_i^4}{r_i^4}-3465\frac{x_i^4+y_i^4}{r_i^4}\left(13\frac{z_i^2}{r_i^2}-1\right)$$

$$+3003\frac{x_i^6+y_i^6}{r_i^6}\left(15\frac{z_i^2}{r_i^2}-1\right)\Bigg]+93(1+\delta)^2\Bigg[-112+2646\frac{z_i^2}{r_i^2}-8316\frac{z_i^4}{r_i^4}+6006\frac{z_i^6}{r_i^6}$$

$$+231\frac{x_i^4+y_i^4}{r_i^4}\left(1-26\frac{z_i^2}{r_i^2}+65\frac{z_i^4}{r_i^4}\right)\Bigg]-[37(1+\delta)^2-31/2]\Bigg[119\left(9\frac{z_i^2}{r_i^2}-1\right)-231\left(2-45\frac{z_i^2}{r_i^2}+99\frac{z_i^4}{r_i^4}\right)$$

$$+441\left(12\frac{z_i^2}{r_i^2}-99\frac{z_i^4}{r_i^4}+143\frac{z_i^6}{r_i^6}\right)-231\left(30\frac{z_i^4}{r_i^4}-169\frac{z_i^6}{r_i^6}+195\frac{z_i^8}{r_i^8}\right)-693\frac{x_i^4+y_i^4}{r_i^4}\left(-1+26\frac{z_i^2}{r_i^2}-65\frac{z_i^4}{r_i^4}\right)\Bigg]$$

$$+[31(1+\delta)^4-17(1+\delta)^6]\Bigg[35\left(9\frac{z_i^2}{r_i^2}-1\right)-105\left(2-45\frac{z_i^2}{r_i^2}+99\frac{z_i^4}{r_i^4}\right)+315\left(12\frac{z_i^2}{r_i^2}-99\frac{z_i^4}{r_i^4}+143\frac{z_i^6}{r_i^6}\right)$$

$$-231\left(30\frac{z_i^4}{r_i^4}-169\frac{z_i^6}{r_i^6}+195\frac{z_i^8}{r_i^8}\right)\Bigg]\Bigg\}.$$

TABLE III. Contributions of various multipoles and shells to the field gradient.

Neighbor shell	$n=2$	$n=4$	$n=6$	Total
1	+0.0421	+0.0533	−0.0093	+0.0862
2	−0.0218	+0.0029	−0.0003	−0.0193
3	+0.0091	−0.0015	⋯	+0.0076
Sum	+0.0294	+0.0547	−0.0096	+0.0745

Numerical evaluation of these terms for the three nearest-neighbor shells gives the results of Table III. The field gradient numbers are expressed in units of $Ze(2/a)^3$. The calculation was done for $c/a=1.078$. Note the rapid convergence with increasing shell radius.

The field gradient arising from the uniform conduction electron distribution in the polyhedron centered at the origin involves the integral

$$\int\rho_e\frac{3z^2-R^2}{R^5}d\mathbf{R}$$

over this polyhedron. The integral can be slightly simplified by the following scheme:

$$\int\rho_e\frac{3z^2-R^2}{R^5}d\mathbf{R}$$

$$=\int_0^{a/4}dy\int_y^{\frac{1}{2}a-y}dx\int_{(\frac{1}{2}a-x)}^{(1+\delta)(\frac{1}{2}a-x)}dz(16\rho_e)\left(\frac{3z^2-R^2}{R^5}\right)$$

$$=\int_0^{a/4}dy\int_0^{\frac{1}{2}a-y}16\rho_e\Bigg\{\frac{(\frac{1}{2}a-x)(1+\delta)}{[x^2+y^2+(\frac{1}{2}a-x)^2(1+\delta)^2]^{\frac{3}{2}}}$$

$$-\frac{(\frac{1}{2}a-x)}{[x^2+y^2+(\frac{1}{2}a-x)^2]^{\frac{3}{2}}}\Bigg\}dx. \quad (4a)$$

The double integral is evaluated numerically; the result is $-0.1144Ze(2/a)^3$. When added to the value $+0.0745Ze(2/a)^3$ from Table III, the result is $-0.319Ze/a^3$.